REPORT DOCUMENTATION PAGE

Form Approved
OMB No. 0704-0188

1. REPORT DATE *(DD-MM-YYYY)*
30-Sep-2009

2. REPORT TYPE
REPRINT

3. DATES COVERED *(From - To)*

4. TITLE AND SUBTITLE
UNIFIED REGIONAL TOMOGRAPHY AND SOURCE MOMENT TENSOR INVERSIONS BASED ON FINITE-DIFFERENCE STRAIN GREEN TENSOR DATABASES

5a. CONTRACT NUMBER
FA8718-06-C-0014

5b. GRANT NUMBER

5c. PROGRAM ELEMENT NUMBER
62601F

6. AUTHOR(S)
Yang Shen[1], Wei Zhang[1], Zhigang Zhang[1], Li Zhao[2], and Xiaoping Yang[3]

5d. PROJECT NUMBER
1010

5e. TASK NUMBER
SM

5f. WORK UNIT NUMBER
A1

7. PERFORMING ORGANIZATION NAME(S) AND ADDRESS(ES)

Science Applications International Corporation
10260 Campus Point Drive
San Diego, CA 92121-1152

8. PERFORMING ORGANIZATION REPORT NUMBER

9. SPONSORING / MONITORING AGENCY NAME(S) AND ADDRESS(ES)
Air Force Research Laboratory
29 Randolph Road
Hanscom AFB, MA 01731-3010

10. SPONSOR/MONITOR'S ACRONYM(S)
AFRL/RVBYE

11. SPONSOR/MONITOR'S REPORT NUMBER(S)
AFRL-RV-HA-TR-2009-1065

12. DISTRIBUTION / AVAILABILITY STATEMENT
Approved for Public Release; Distribution Unlimited.

Science University of Rhode Island[1], Institute of Earth Sciences, Academia Sinica, Taiwan[2],and Science Applications International Corporation[3]

13. SUPPLEMENTARY NOTES
Reprinted from: Proceedings of the 2009 Monitoring Research Review – Ground-Based Nuclear Explosion Monitoring Technologies, 21 – 23 September 2009, Tucson, AZ, Volume I pp 201 - 210.

14. ABSTRACT

Seismic monitoring requires accurate source characterization in real time. Accurate 3D earth models are essential for accurate predictions of seismic observables and source characterization. While recovering the true earth structure has always been the goal of tomographic inversions, methods based on full wavefields in 3D reference models have several distinct advantages. Made possible by advances in high-performance computation, this full-wave approach accounts for complex wave propagation in 3D heterogeneous earth, enables fuller utilization of seismic records, and allows us to linearize the inverse problem by iteratively updating the 3D reference model. An important benefit of physically realistic and accurate modeling of wavefields in 3D models is the consistency of the system of equations in inversion. This is particularly important for the integration of different types of observations (*P*, *S*, and surface waves including empirical Green's functions derived from ambient noise) in inversion. Two methods have been developed in this field to carry out full-wave tomography iteratively with 3D reference models. One is the adjoint-wavefield (AW) method, which back-propagates the data from the receivers to image the structure. The other is the scattering-integral (SI) method, which constructs the strain Green tensor (SGT) databases and calculates sensitivity kernels for each data functional. Both methods are based on the full-wave theory, and the main differences are in the computational approaches. In general, the adjoint method is CPU intensive, while the SGT-database approach requires a large disk space and fast network. To date, the AW and SI methods use two different approaches in calculating synthetic waveforms, i.e. the spectral-element method and finite-difference (FD) method, respectively. One notable advantage of the SI method is that the SGT databases make it possible to use 3D synthetics in real time seismic monitoring.

We have systematically developed a unified source mechanism and tomographic inversion method based on 3D finite-difference SGT (FDSGT) databases. The main developments include:

- a finite-difference code in the spherical coordinate system for regional and global wave propagation;
- a new and efficient implementation of the Perfectly Matched Layer that provides a better performance for waves incident at a near-grazing angle, low frequency waves or evanescent waves;
- accurate representation of *Pn*/*Sn* finite-frequency sensitivity kernels;
- a fuller utilization of an arrival on all three components of seismic records;
- the dependence of *P* waveforms on *S*-wave speed anomalies and Rayleigh waveforms on *P* wave speed anomalies;
- moment tensor inversion using SGT databases; and
- joint *P* and *S* velocity tomography using an integrated body and surface wave dataset.

We have applied this method to Iran and the southeast Tibetan plateau and demonstrated our SGT-based, unified tomography and moment tensor inversion. The FDSGT moment tensor solutions agree well with the global centroid moment tensors (GCMT). Because of local/regional stations, 3D models, and shorter-period waves than in GCMT, FDSGT moment tensor solutions provide better locations, particularly in constraining depth. The joint *P* and *S* velocity model of the southeast Tibetan plateau from tomography of ~10,000 finite-frequency body and surface wave measurements shows an unprecedented resolution compared to previous models and tomography of similar scales.

15. SUBJECT TERMS
Finite-frequency tomography, Moment tensors, Finite difference

16. SECURITY CLASSIFICATION OF:			17. LIMITATION OF ABSTRACT	18. NUMBER OF PAGES	19a. NAME OF RESPONSIBLE PERSON
a. REPORT	b. ABSTRACT	c. THIS PAGE			Robert J. Raistrick
UNCLAS	UNCLAS	UNCLAS	SAR	10	19b. TELEPHONE NUMBER *(include area code)*

UNIFIED REGIONAL TOMOGRAPHY AND SOURCE MOMENT TENSOR INVERSIONS BASED ON FINITE-DIFFERENCE STRAIN GREEN TENSOR DATABASES

Yang Shen[1], Wei Zhang[1], Zhigang Zhang[1], Li Zhao[2], and Xiaoping Yang[3]

University of Rhode Island[1], Institute of Earth Sciences, Academia Sinica, Taiwan[2], and Science Applications International Corporation[3],

Sponsored by the Air Force Research Laboratory

Award No. FA8718-06-C-0014
Proposal No. BAA06-60

ABSTRACT

Seismic monitoring requires accurate source characterization in real time. Accurate 3D earth models are essential for accurate predictions of seismic observables and source characterization. While recovering the true earth structure has always been the goal of tomographic inversions, methods based on full wavefields in 3D reference models have several distinct advantages. Made possible by advances in high-performance computation, this full-wave approach accounts for complex wave propagation in 3D heterogeneous earth, enables fuller utilization of seismic records, and allows us to linearize the inverse problem by iteratively updating the 3D reference model. An important benefit of physically realistic and accurate modeling of wavefields in 3D models is the consistency of the system of equations in inversion. This is particularly important for the integration of different types of observations (*P*, *S*, and surface waves including empirical Green's functions derived from ambient noise) in inversion.

Two methods have been developed in this field to carry out full-wave tomography iteratively with 3D reference models. One is the adjoint-wavefield (AW) method, which back-propagates the data from the receivers to image the structure. The other is the scattering-integral (SI) method, which constructs the strain Green tensor (SGT) databases and calculates sensitivity kernels for each data functional. Both methods are based on the full-wave theory, and the main differences are in the computational approaches. In general, the adjoint method is CPU intensive, while the SGT-database approach requires a large disk space and fast network. To date, the AW and SI methods use two different approaches in calculating synthetic waveforms, i.e. the spectral-element method and finite-difference (FD) method, respectively. One notable advantage of the SI method is that the SGT databases make it possible to use 3D synthetics in real time seismic monitoring.

We have systematically developed a unified source mechanism and tomographic inversion method based on 3D finite-difference SGT (FDSGT) databases. The main developments include:

- a finite-difference code in the spherical coordinate system for regional and global wave propagation;
- a new and efficient implementation of the Perfectly Matched Layer that provides a better performance for waves incident at a near-grazing angle, low frequency waves or evanescent waves;
- accurate representation of *Pn*/*Sn* finite-frequency sensitivity kernels;
- a fuller utilization of an arrival on all three components of seismic records;
- the dependence of *P* waveforms on *S*-wave speed anomalies and Rayleigh waveforms on *P*-wave speed anomalies;
- moment tensor inversion using SGT databases; and
- joint *P* and *S* velocity tomography using an integrated body and surface wave dataset.

We have applied this method to Iran and the southeast Tibetan plateau and demonstrated our SGT-based, unified tomography and moment tensor inversion. The FDSGT moment tensor solutions agree well with the global centroid moment tensors (GCMT). Because of local/regional stations, 3D models, and shorter-period waves than in GCMT, FDSGT moment tensor solutions provide better locations, particularly in constraining depth. The joint *P* and *S* velocity model of the southeast Tibetan plateau from tomography of ~10,000 finite-frequency body and surface wave measurements shows an unprecedented resolution compared to previous models and tomography of similar scales.

OBJECTIVES

The objeetives of this work are to obtain Finite-Frequency Seismic Tomography (FFST) velocity models for Eurasia and to refine crustal and shallow upper mantle velocity and attenuation models for focused areas of interest.

RESEARCH ACCOMPLISHED

Accurate 3D earth models are essential for accurate predictions of seismic observables and source characterization. While reeovering the true form and magnitude of earth structures has always been the goal of tomographic inversions, recent studies show that methods based on full wavefields in 3D reference models have several distinct advantages in relating seismic observations to highly heterogeneous Earth structures. Made possible by advances in high-performance computation, this full-wavefield approach accounts for complex wave propagation in 3D heterogeneous Earth (Zhao et al., 2005; Tromp et al., 2005; Liu and Tromp, 2006; Zhang et al., 2007), enables fuller utilization of an arrival on all three components of seismic records (Shen et al., 2008a), and allows us to linearize the inverse problem by iteratively updating the 3D reference model. An important benefit of physically realistic and accurate modeling of full wavefields in 3D models is the consistency of the system of equations in inversion. This is particularly important for the integration of different types of observations (*P*, *S*, surface waves including empirical Green's functions derived from ambient noise) in inversion, which is an essential step to obtain a coherent and self-consistent model of the crust and mantle. Seismic tomography based on path- or structure-averaging (rays) and 1D or 2D reference models does not accurately place the 3D sensitivities of seismic observations in a complex 3D model. The mismatch in sensitivities due to approximations in theory becomes problematic when the target resolutions are at scales smaller than the Fresnel zone. For scale, a 1–Hz *Pn* wave recorded by a receiver ~1000 km from the source has a Fresnel zone width of ~200 km in the middle of the wave path (Zhang et al., 2007). van der Lee and Frederiksen (2005) recognize that a more consistent and linear system of equations offered by the full-wavefield approach would fit the combined datasets better under comparable regularization biases.

Two methods have been developed to carry out full-wave tomography iteratively with 3D reference models. One is the AW method, which back-propagates the data from the receivers to image structure (Tromp et al., 2005; Liu and Tromp, 2006). The other is the SGT-based, SI method, which calculates and stores the sensitivity kernels for each data functional (Zhao et al., 2005; Zhang et al., 2007). Both methods are based on the full wave theory. The main differences are in the computational approaches. In general, the adjoint method is CPU intensive, while the SGT database approach requires a large disk spaee and a fast network. A notable advantage of the SI method is that it provides both the Hessian and gradient of the misfit funetion in the tomographie inversion and requires a fewer number of simulations per model iteration to achieve the same level of data variance reduction (Chen et al., 2007). The SGT databases can also be used in source moment tensor inversions, making it possible to use 3D synthetics in real time seismic monitoring. To date, the AW and SI methods use two different approaches to calculate synthetic waveforms: the spectral-element method (SEM) (Komatitsch et al., 2002) and finite-difference method (Olsen, 1994; Zhang et al., 2008; Zhang and Shen, 2009; Zhang et al., 2009), respectively.

Unified tomography and source inversions based on finite-difference SGT database

In the SGT-based approach, the displacement can be expressed as (Zhao et al., 2006):

$$\begin{aligned} u_n(\mathbf{r};\mathbf{r}_s) &= \partial_i^s G_{nj}(\mathbf{r};\mathbf{r}_s) M_{ji} \\ &= \frac{1}{2}[\partial_i^s G_{jn}(\mathbf{r}_s;\mathbf{r}) + \partial_j^s G_{in}(\mathbf{r}_s;\mathbf{r})] M_{ji} \\ &= H_{ijn}(\mathbf{r}_s;\mathbf{r}) M_{ji} \end{aligned} \tag{1}$$

where $\mathbf{r}$ is the location vector, $\mathbf{r}_s$ is the source location, M_{ji} the moment tensor component (i,j=1-3), $G(\mathbf{r};\mathbf{r}_s)$ and $G(\mathbf{r}_s;\mathbf{r})$ the Green tensors for a unit impulsive force at the source and $\mathbf{r}$, respectively, and $H_{ijn}(\mathbf{r}_s;\mathbf{r})$ the strain Green tensor composed of the spatial gradient of the Green tensors. The subscript n denotes the component of the displaeement. The source-receiver reciprocity and the symmetry of the moment tensor have been applied in Equation (1). Notice the SGT can be at any location in the medium and thus can also be at the receiver location $\mathbf{r}_R$. Equation (1) is the basis upon which the FDSGT moment tensor inversions are developed (Zhao et al., 2006; Shen et al., 2009).

The waveform change at $\mathbf{r}_R$ due to a local model perturbation at an arbitrary position $\mathbf{r}$, can be expressed as (Zhao et al., 2006):

$$\delta u_n(\mathbf{r}_R;\mathbf{r}_s) = H_{ijn}(\mathbf{r};\mathbf{r}_R)\delta C_{ijkl}(\mathbf{r})\varepsilon_{lk}(\mathbf{r};\mathbf{r}_s) \quad (2)$$

where $\delta C_{ijkl}(\mathbf{r})$ is the perturbation of the elasticity tensor and $\varepsilon_{lk}(\mathbf{r};\mathbf{r}_s)$ is spatial gradient elements of the displacement vector, which requires one forward wave simulation from the source. The total waveform change due to the model perturbation in the entire volume can be found by volume integration of Equation (2) in the model. The above waveform perturbation equation is the essential ingredient in the SGT-based tomographic method. The Fréchet kernels relating elastic and anelastic properties to any seismic data, such as frequency-dependent traveltime and amplitude anomalies, can be obtained from it (Zhao et al., 2005; Zhang et al., 2007).

Figure 1 is a schematic illustration of the unified tomography and source moment tensor inversion based on 3D FDSGT databases. Station SGT databases are constructed from 3D reference models by finite-difference simulation of the responses to orthogonal unit impulsive point forces acting at the stations. The SGTs in a small volume surrounding the source reference location extracted from the databases make it possible to invert for source moment tensors and location in a global optimization scheme. Forward wave propagation simulation from the source in the 3D reference model provides synthetic waveforms at the station and within the entire model. Travel time, amplitude, or waveform anomalies are measured from the observed and synthetic waveforms at stations. The forward wave field (from the source) and the station SGTs are used to calculate the finite-frequency sensitivities to perturbations in V_p, V_s (or bulk and shear moduli), density, and attenuation. Together with the sensitivities to source parameters, the measurements and structural sensitivity kernels are used to invert for the earth structure. The inversion results are added to the 3D reference model. This process can be repeated to progressively improve the resolution.

Source characterization and construction of hierarchical FDSGT databases

Most earthquake source studies to date utilize 1D earth models in the calculation of synthetic waveforms or Green's functions. To accommodate 3D structural heterogeneities, segments of body and surface waves are time-shifted before waveform fitting (e.g., Zhao and Helmberger, 1994; Zhu and Helmberger, 1996). In places with highly heterogeneous structure, this "cut-and-paste" of waveform segments may not fully account for the complexity of wave phenomena caused by 3D structures (e.g., wave focusing/defocusing). One of the major sources of errors in moment tensor inversion is phase skipping between the observed and synthetic waveforms. When traveltime delays due to 3D velocity heterogeneities are comparable to the wave period, phase skipping becomes a challenging problem.

Advance in computation has made the use of 3D Green's functions in earthquake source inversion an increasingly attractive option in routine operation. Liu et al. (2004) determined the source mechanisms of small to moderate earthquakes in southern California using synthetic waveforms calculated with the spectral-element method. Because the derivatives of the source parameters are determined numerically by differentiating synthetics with respect to the source parameters, up to 10 forward simulations are needed for each earthquake (six moment tensor components, latitude, longitude, depth, and the reference location). When the reference location is far from the true location, the derivatives of the location parameters may not adequately reflect the non-linear variation of waveforms as a function of location. Taking advantage of the source-receiver reciprocity, Zhao et al. (2006) introduced the use of strain Green's tensor in source inversion based on 3D reference models. We have extended the SGT-database approach to regional and teleseismic scales (Shen et al., 2009), so we are able to use any combination of local and teleseismic waveforms in source inversion. We fit filtered and time-shifted waveforms directly. For a given source location, the waveforms are linear functions of the moment tensor elements, which can be solved as a linear inverse problem. To account for perturbations in earthquake source location, we carry out a grid search in the vicinity of the reference location.

Figure 2 shows the selected earthquakes in the southeast Tibetan plateau and the stations used in moment tensor inversion (Shen et al., 2009). We calculate synthetic waveforms using a non-staggered grid finite-difference code in a polar-spherical coordinate system (Zhang et al., 2009). Wave simulations are carried out on three geographical scales: local/near regional, far regional, and teleseismic. An updated crust and upper mantle model (CUB 2.0, Shapiro and Ritzwoller, 2002) is used as the 3D reference model. The FDSGT moment tensors agree well with the global centroid moment tensor (GCMT) solutions (Figure 3), with one notable exception at the eastern Himalayan syntaxis (event 03.230 in Figure 3). The GCMT solution shows a strike-slip event at 33 km depth, while our FDSGT solution is a shallow (2±16 km) thrust event.

Figure 4 shows an example of the fit between the observed waveforms and the synthetics calculated from the FDSGT databases. An inspection of the waveforms in detail (Shen et al., 2009) shows that the regional stations, the 3D model, and shorter-period body waves than those used in the GCMT solutions tend to provide tighter constraints on the source location, particularly the depth.

Full-wave tomography and finite-frequency kernels based on 3D reference models

To date the inversions of *P*- and *S*-wave speeds have been carried out separately under the assumption that *P* traveltimes are affected only by the *P*-wave speed of the elastic media and *S* traveltimes by the *S*-wave speed. The practice stems from ray theory, in which *P* and *S* waves are completely decoupled except for conversions at discontinuities following the Snell's law. Based upon numerical and analytical solutions, we have shown that for finite-frequency waves, *S*-speed perturbation may have significant effects on *P* waveforms (Zhang and Shen, 2008). At places near the source or receiver, the cross-dependence of *P* waveforms on *S*-speed perturbation is substantial. For example, the integrated absolute *P*-traveltime sensitivity to *S*-speed perturbation is 31% of that to *P*-speed perturbation when the source-receiver distance is seven times the wavelength ($L/\lambda=7$, where λ is the wavelength and *L* the distance to the receiver). At a source-receiver distance of 100 wavelengths, the ratio is about 5%. This finite-frequency effect has important implications for seismic tomography, particularly at regional and local scales, where target structures are often located within several tens of wavelengths from receivers or from both sources and receivers. Even for regions far from sources and receivers, neglecting this cross-dependence means that the estimates of the *P* speed near the source and receiver are likely biased and such errors may propagate into the rest of the model in tomographic inversion.

Figure 5 shows the phase sensitivities of a regional Rayleigh wave to *S*- and *P*-wave speeds. Similar to the results for southern California in Liu and Tromp (2006), there are large 3D variations in the finite-frequency kernels due to wave-speed variations. Although commonly neglected in surface wave tomography, *P*-wave speed (and density) affects Rayleigh waves (also see Zhou et al. (2004) and Liu and Tromp (2006)). The maximum sensitivity to *P*-wave speed is on the surface and at a level comparable to the Vs kernel. It decreases to ~10% of the maximum at depth of $\sim\lambda/4$. Since the peak of the Vs sensitivity is at the depth of $\sim\lambda/3$ and heterogeneities in the mantle are generally much weaker than in the crust, it may be necessary to include the sensitivities to *P*-speed and density for long-period (~50+ s) Rayleigh waves in a high-resolution inversion. When integrated with *Pn*, *Sn*, and Love waves, Rayleigh waves may provide additional constraints on the *P*-wave structure in the crust. At the very least, incorporating the effects of *P*-speed on Rayleigh waves may minimize a likely cause contributing to the apparent Love-Rayleigh discrepancy and radial anisotropy.

Figure 6a and 6b show the *P* and *S* wave velocities, respectively, of the shallow crust of the southeast Tibetan plateau. The model is derived from a joint inversion of ~10,000 measurements of phase anomalies of *P*/*Pn*, *S*/*Sn* and Rayleigh/Love waves in three frequency bands ranging from 0.008–0.1 Hz (Shen et al., 2008b). After two iterations, the combined velocity anomalies relative to the initial reference model (CUB 2.0, Shapiro and Ritzwoller, 2002) show that the observations require P velocity increases just north of the Indus Yalu suture (IYS), near the Bangong-Nujiang suture (BNS), and west of the Xianshuhe Fault system (XSHF). These high-velocity anomalies correlate well with areas of granitic and/or more metamorphosed Proterozoic and Paleozoic rocks among the regional Mesozoic background (Geological map of the Tibetan plateau, China Academy of Geological Sciences, Chengdu). The P-wave resolution at such a shallow depth is attributed in part to the sensitivity of Rayleigh waves to *P*-wave speed perturbations (Figure 5). The updated *S*-velocity model (Figure 6b) shows a sharp velocity contrast that follows the boundary of the Tibetan plateau as outlined by the 1000 m elevation contour.

CONCLUSIONS AND RECOMMENDATIONS

We have developed a unified tomography and earthquake moment-tensor inversion based on 3D reference models. The new approach accounts for complex wave propagation, enables fuller utilization of an arrival on all three components of seismic records, and linearizes the inverse problem by iteratively updating the 3D reference model. We calculate synthetic waveforms using a non-staggered grid finite-difference code in a polar-spherical coordinate system. The new moment tensor solutions accommodate the 3D velocity heterogeneities and are an integral part of the unified tomography and source inversion. Body and surface wave traveltimes are inverted jointly for *P* and *S* wave speed perturbations. The results show a much-improved resolution compared to the reference model and regional models of similar scale.

ACKNOWLEDGEMENTS

Dr. Eric Engdahl provided data used to construct portions of Figure 4.

REFERENCES

Chen, P., T. H. Jordan, and L. Zhao (2007). Full three-dimensional tomography: a comparison between the scattering-integral and adjoint-wavefield methods, *Geophys. J. Int.* 170: 175–181.

Komastitsch, D., J. Ritsema, and J. Tromp (2002). The spectral-element method, Beowulf computing, and global seismology, *Science* 298: 1737–1742.

Liu, Q., J. Polet, D. Komatitsch, and J. Tromp (2004). Spectral-element moment tensor inversions for earthquakes in southern California, *Bull. Seism. Soc. Am.* 94: 1748–1761.

Liu, Q., and J. Tromp (2006). Finite-frequency kernels based on adjoint methods, *Bull. Seismol. Soc. Am.* 96: 2383–2397.

Olsen, K. B. (1994). Simulation of three-dimensional wave propagation in the Salt Lake Basin, Ph.D. Thesis, University of Utah, Salt Lake City, Utah, 157 p.

Shapiro, N. M. and M. H. Ritzwoller (2002). Monte-Carlo inversion for a global shear velocity model of the crust and upper mantle, *Geophys. J. Int.* 151: 88–105.

Shen, Y., Z. Zhang, and W. Zhang (2009). Moment inversions of earthquakes in the southeast Tibetan plateau using finite-difference strain Green tensor database, submitted to *Geophys. J. Int.*

Shen, Y., Z. Zhang, and L. Zhao (2008a). Component-dependent Fréchet sensitivity kernels and utility of three-component seismic records, *Bull. Seism. Soc. Am.* 98: doi:10.1785/0120070283.

Tromp, J., C. Tape, and Q. Liu (2005). Seismic tomography, adjoint methods, time reversal and banana-doughnut kernels, *Geophys. J. Int.* 160: 195–216.

van der Lee, S. and A. Frederiksen (2005). Surface wave tomography applied to the north American upper mantle, in Seismic Earth: Array Analysis of Broadband Seismograms, Geophys. Monograph Ser. 157, AGU, 67–80.

Zhang, W. and Y. Shen (2009). Unsplit Complex Frequency Shifted PML Implementation Using Auxiliary Differential Equation for Seismic Wave Modeling, submitted to *Geophysics*.

Zhang, W., Y. Shen, and X. Chen (2008). Numerical simulation of strong ground motion for the Ms8.0 Wenchuan earthquake of 12 May 2008, *Sci. China Ser. D-Earth Sci.* 51: 1673–1682

Zhang, W., Y. Shen, and L. Zhao (2009). 3D seismic wave modeling in spherical coordinate by a non-staggered finite difference method, manuscript in preparation.

Zhang, Z. and Y. Shen (2008). Cross-dependence of finite-frequency compressional waveforms to shear seismic wave-speeds, *Geophys. J. Int.* 174: doi:10.1111/j.1365-246X.2008.03840.x.

Zhang, Z., Y. Shen, and L. Zhao (2007). Finite-frequency sensitivity kernels for head waves, *Geophys. J. Int.* 171: 847–856.

Zhao, L., P. Chen, and T. H. Jordan (2006). Strain Green tensor, reciprocity, and their applications to seismic source and structure studies, *Bull. Seism. Soc. Am.* 96: doi:10.1785/0120050253.

Zhao, L., T. H. Jordan, K. B. Olsen, and P. Chen (2005). Fréchet kernels for imaging regional earth structure based on three-dimensional reference models, *Bull. Seism. Soc. Am.* 95: 2066–2080.

Zhao, L. and D. V. Helmberger (1994). Source estimation from broadband regional seismograms, *Bull. Seism. Soc. Am.* 84: 91–104.

Zhou, Y., F. A. Dahlen, and G. Nolet (2004). 3-D sensitivity kernels for surface-wave observables, *Geophys. J. Int.* 158: 142–168.

Zhu, L. and D. V. Helmberger (1996). Advancement in source estimation techniques using broadband regional seismograms, *Bull. Seism. Soc. Am.* 86: 1634–1641.

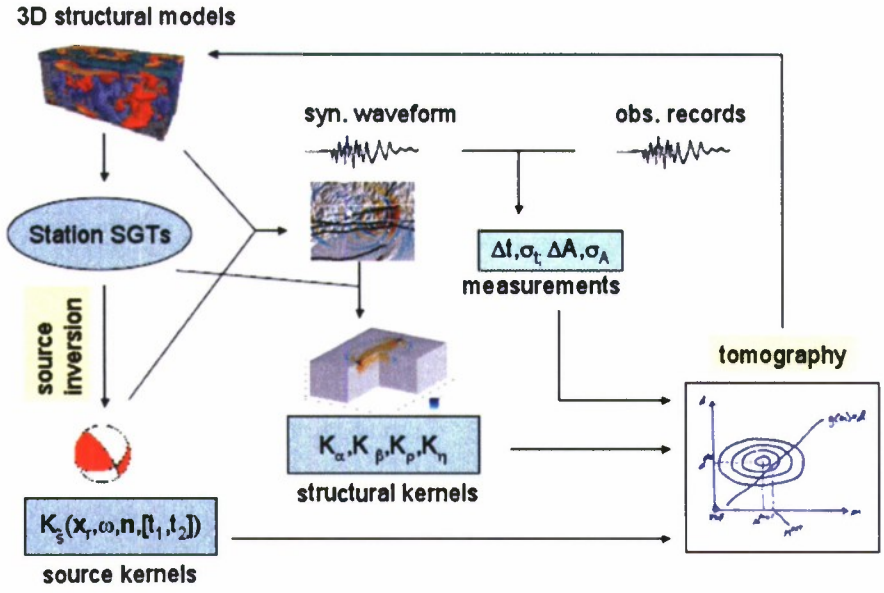

Figure 1. Schematic illustration of the unified tomography and moment tensor inversions based on 3D FDSGT databases.

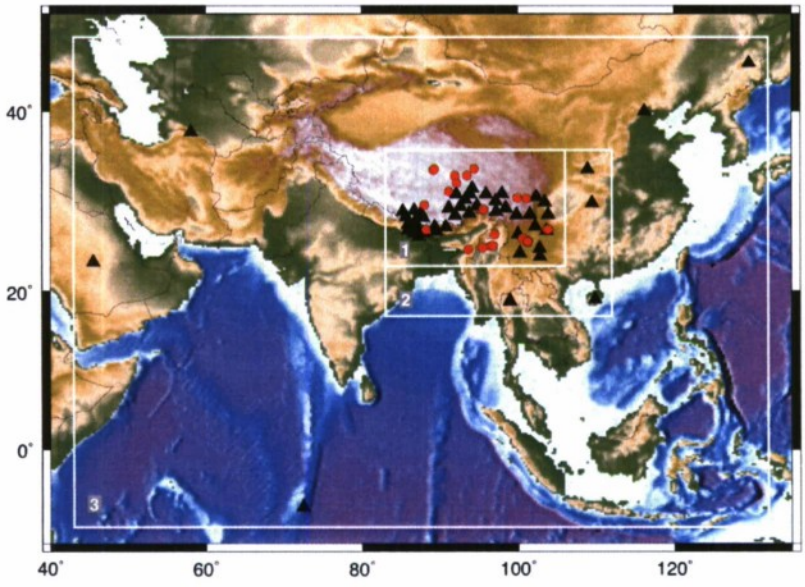

Figure 2. Selected earthquakes (red circles) in the southeast Tibetan plateau during 2001–2004 and the stations (black triangles) used in moment tensor inversions. White rectangles outline the three geographic scales of the finite-difference wave simulation: (1) local/near regional, (2) far-regional, and (3) teleseismic.

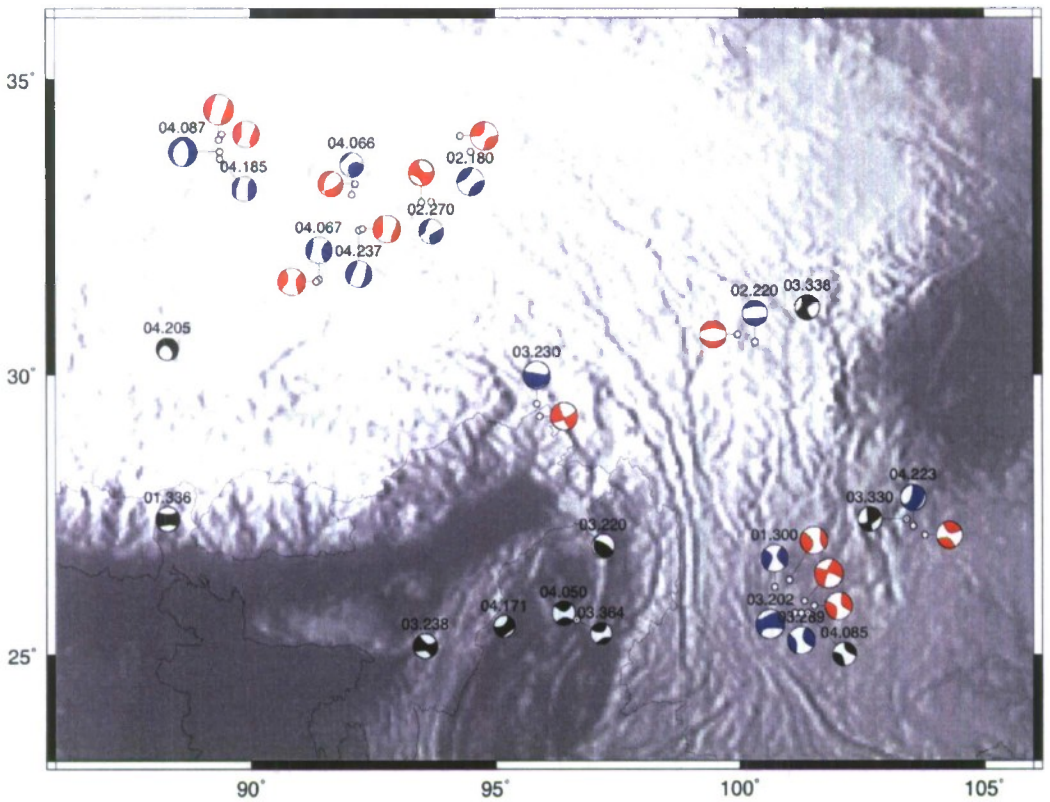

Figure 3. Comparison of the FDSGT (white-and-blue symbols) and GCMT (white-and-red symbols) solutions for 13 earthquakes during 2001–2004 in the southeast Tibetan plateau. The numbers above the FDSGT solution denote the year and Julian day of the earthquake. Also plotted are the source mechanisms of 10 additional earthquakes without GCMT solutions (black-and-white symbols).

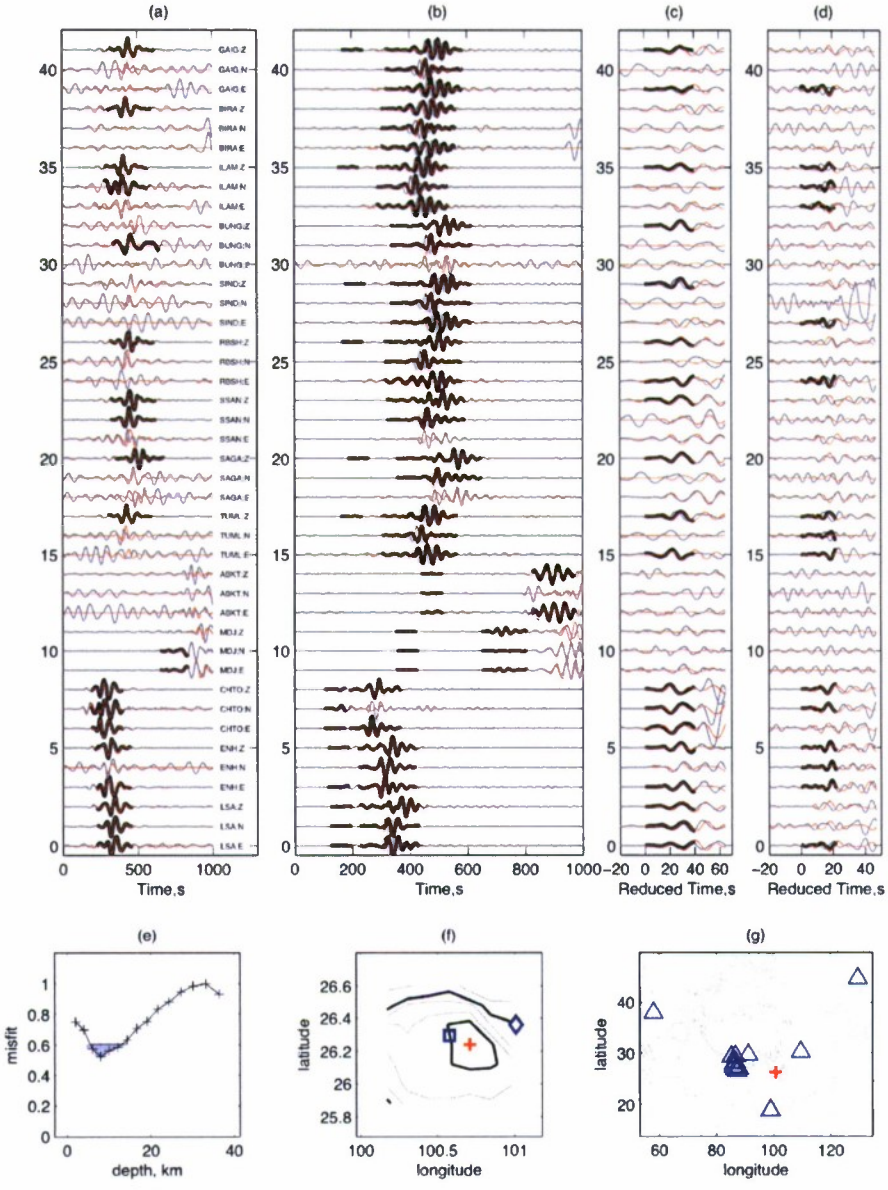

Figure 4. (a–d) Observed waveforms (thick gray lines) are compared with the synthetics for the best source moment tensor solution (red lines). The frequency bands are, from left to right, 0.00833–0.0167, 0.0167–0.0333, 0.0333–0.0667, and 0.0667–0.167 Hz. Dark thick lines are time-shifted observed waveforms used in the final inversion. For the first arrivals (in c and d), the time is reduced to align the arrivals within the time window. The amplitude is normalized by individual trace. (e) Normalized waveform misfit as a function of depth. Crosses mark the grid-search depths. The shaded region indicates the 1σ confidence limit. (f) Contours of various confidence limits at the depth of the global best solution (8 km for this event). The cross marks the FDSGT location; the square is the EHB location (Engdahl, see acknowledgements); and the diamond is the global centroid moment tensor location. From the innermost contour surrounding the FDSGT solution, the contours are the 68% (dark line), 80%, 90%, 95% (dark line), and 99% confidence limits. (g) Triangles and cross mark the stations used in the source inversion and the event, respectively. Gray contours follow 0, 2000 and 4000 m elevation.

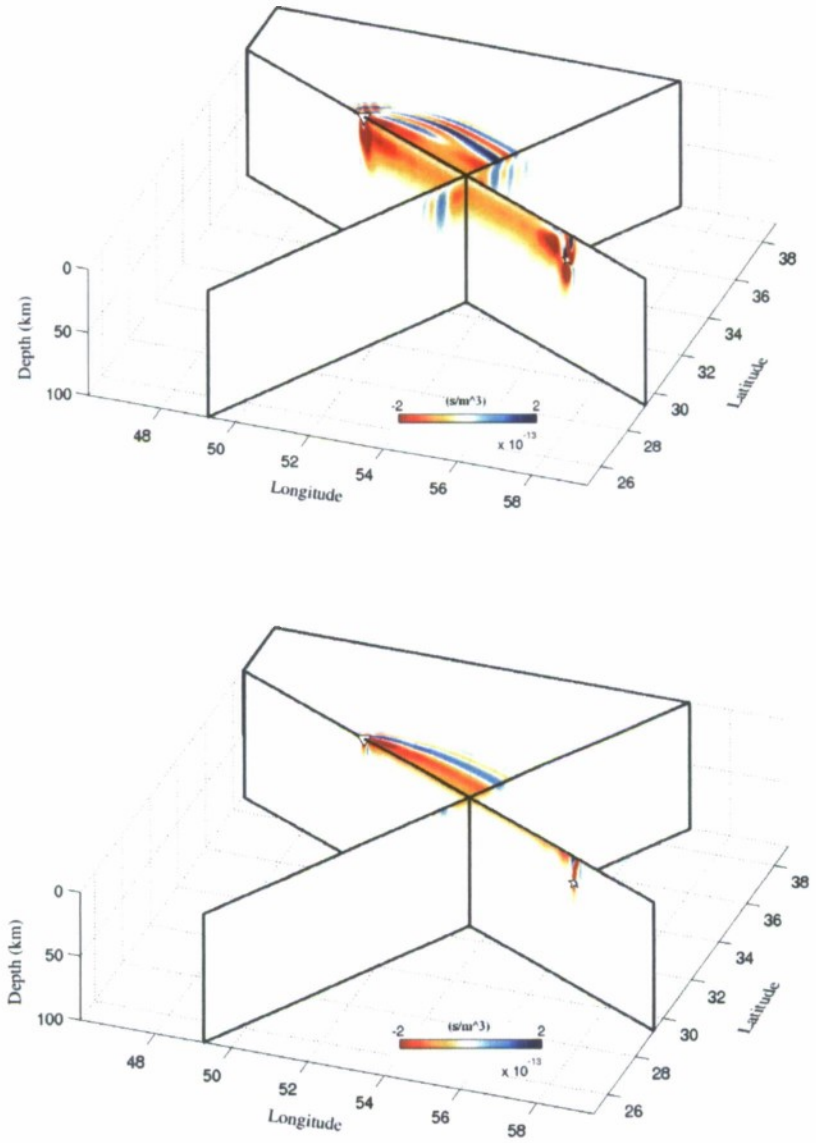

Figure 5. Phase sensitivity kernels of a regional Rayleigh wave to *S* wave-speed (top) and *P* wave-speed (bottom) perturbations relative to a 3D referenee model. The period of the wave is 10–20 s. The two vertieal eross-seetions eut the model along the great eirele path between the earthquake souree (in the southeast eorner of the model) and reeeiver (in the northwest eorner of the model) and perpendieular to the great eirele. Also shown is a quadrant of a horizontal seetion on the surfaee. The seale is $\pm 2 \times 10^{-13}$ s/m^3.

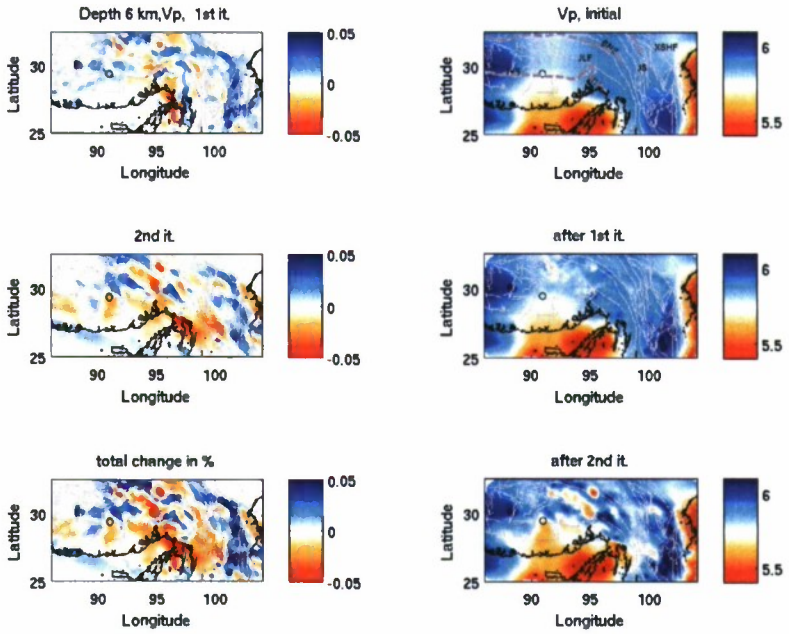

Figure 6a. *P*-wave velocity variations at 6 km depth in the southeast Tibetan plateau. The initial 3D reference model (top right) is converted from CUB 2.0 by a V_p/V_s ratio of 1.74 in the crust and the V_p/V_s of AK135 in the mantle. The unit of the color bar is km/s. The left panels show the velocity perturbations after the 1st and 2nd iteration and the total velocity change in percent. The middle-right and bottom-right panels show the updated models after the 1st and 2nd iterations. The main tectonic features, the Indus-Yalu suture (IYS), Bangong-Nujiang suture (BNS), and the Xianshuihei Fault system (XSHF), are marked in the upper right panel. The 1000 m elevation contour outlines the southern margin of the Tibetan plateau and the boundary of the Sichuan basin.

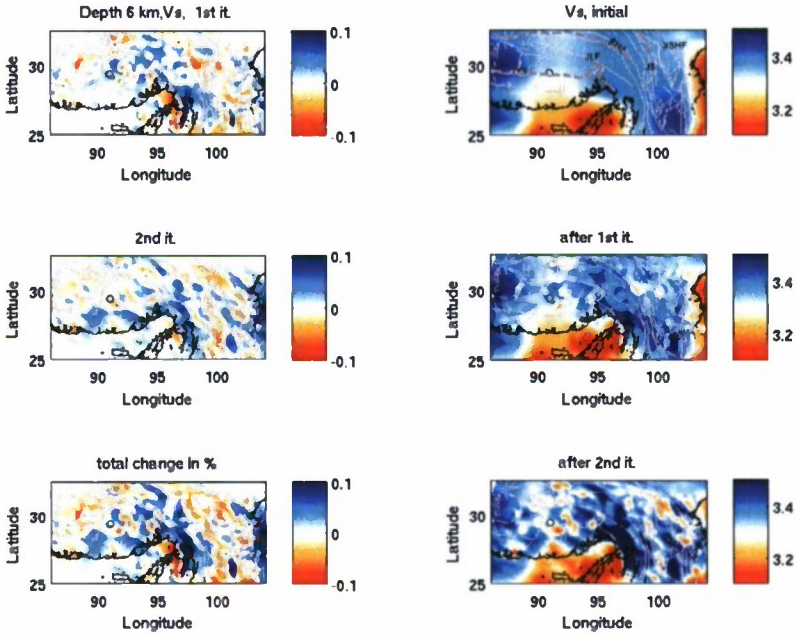

Figure 6b. Same as Figure 6a, except showing *S* velocity.